Journal of Porous Materials (2021) 28:1643–1653
https://doi.org/10.1007/s10934-021-01104-1

Nickel nanoparticles anchored over porous triazine-thiourea-sulfonamide to explore the reduction of carbonyl compounds

Abumuslim Rahimi[1] · Ramin Ghorbani-Vaghei[1] · Sedigheh Alavinia[1]

Accepted: 5 June 2021 / Published online: 25 June 2021

Abstract
In the recent few years, polymer based nanomaterials are emerged as promising candidates in new generation catalysis. In this regard, we report the synthesis of nickel nanoparticles at mild conditions using porous triazine-thiourea-sulfonamide support (TTSA). The novel heterogeneous polymer support was synthesized by silica template method. The synthetically modified porous material (TTSA@Ni NPs) was analyzed in details over a number of physicochemical methods like, FT-IR, FE-SEM, HR-TEM, EDX, XRD, TGA and ICP-OES. In catalytic exploration we aimed the synthesis of alochohols from the reduction of aldehydes/ketones in water. Furthermore, the prepared green heterogeneous catalyst can be recycled and recovered six times without significant loss in the catalytic activity

Keywords Triazine-thiourea-sulfonamide (TTSA) · Mesoporous catalyst · Aldehydes · Ketones · Formic acid/triethyl amine · Ni NPs

1 Introduction

In recent days, the development of environmentally benign protocols has been explored for the synthesis of bioactive heterocycles by eliminating the use of hazardous, expensive solvents and reagents along with multistep reaction course to avoid the formation of unwanted side products [1]. Among the important synthetic methods, the selective reduction of carbonyl compounds has collected remarkable attention [2], because various valuable chemicals can be synthesized from alchohol through condensation, etherification, oxidation, and esterification [3–5]. Due to the remarkable potentially of alcohol in organic synthesis, design and development of nanocomposite for the reduction of carbonyl compounds has been an interesting research among the scientists.

Recent developments in the synthesis of heterogeneous nano catalyst using heterogeneous support have gained considerable curiosity [6–9]. In this context, the use of porous polymer is an exponentially growing research area in modern synthetic chemistry which offers several advantages such as high surface area, high stability (chemical and thermal), easy availability, low cost, high reaction yields with simplified recovery and reusability [10–12]. Along with porous polymer, the synthesis of nickel nano catalysts, applied as a heterogeneous catalyst, has attracted a wide variety of interests in various organic reactions [13]. However, heterogeneous nickel catalysts suffer from some drawbacks such as leaching of metal NPs, which leads to the loss of catalytic activity. Thus, it is very important to prepare an ideal catalyst support with a high surface area, which results in minimizing the mentioned problems.

Sulfonamide scaffolds have attracted the attention of many researchers due to their potential in catalytic applications [14]. The results obtained from catalytic application of sulfonamides indicate that sulphonamides play a vital role in heterogeneous substrate and catalysts [15–22]. In this connection, the use of cross-linked poly sulfonamides as heterogeneous support has been quite familiar derived from their easy and low-cost synthesis, low toxicity, abundance and outstanding isolation followed by reusability. The surface amine and sulfonamide groups additionally help towards the covalent immobilization of the organo-functions [15–22]. As a consequence, we have been prompted to demonstrate a novel material by forming a novel porous cross-linked

✉ Ramin Ghorbani-Vaghei
rgvaghei@yahoo.com; ghorbani@basu.ac.ir

[1] Department of Organic Chemistry, Faculty of Chemistry, Bu-Ali Sina University, Zip Code 65174 Hamedan, Iran

triazine-thiourea-sulfonamide (TTSA) through silica template method and further decorated with in situ generated Ni NPs to have the TTSA@Ni nanocomposite (Scheme 1). Finally, we exploited the novel catalyst in the reduction of aldehydes and ketones to green synthesis of alcohol in excellent yields (Scheme 2).

2 Experimental

2.1 *Synthesis of SiO_2 NPs*

SiO_2 NPs with an average diameter of about 25 nm were prepared according to the Stöber method [23].

2.2 *Synthesis of SiO_2@TTSA*

A mixture of benzene-1,3-disulfonyl chloride (1 mmol, 0.275 g), 1,3,5-triazine-2,4,6-triamine (0.2 mmol, 0.03 g), thiourea (0.7 mmol, 0.05 g) and silica nanoparticles (0.05 g) were taken in 25 mL of dry acetonitrile and refluxed for 12 h. The resulting nanocomposite (SiO_2@TTSA) was filtered off. Finally, it was washed thoroughly with acetonitrile and dried.

2.3 Synthesis of porous TTSA

The mixture of HF solution (10 mL, 10 wt.% in 10 mL deionized water), and deionized water (10 mL) was added

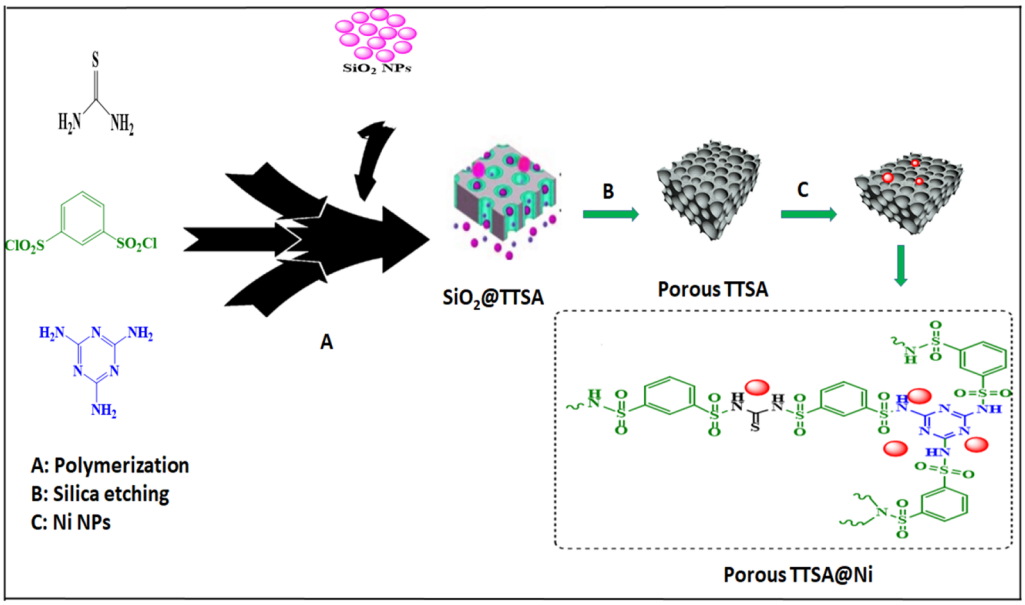

Scheme 1 The general route for the synthesis of mesoporous TTSA@Ni catalyst

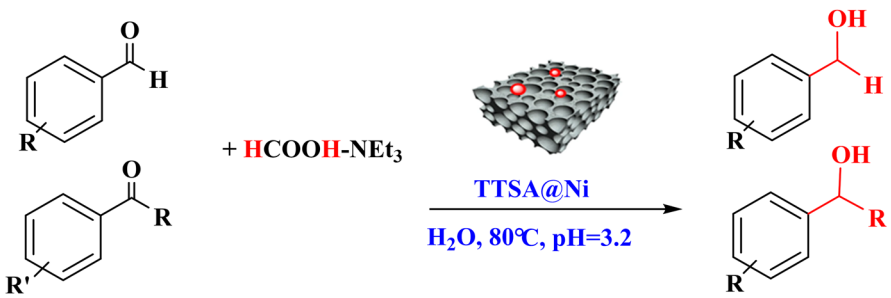

R: H, *p*-Me, *p*-OMe, *p*-Cl, *p*-NO_2, p-F, *p*-$N(Me)_2$, *p*-OH, *m*-OH, *m*-F, Furan, Thiophene, Indole

R': H, *p*-Me, *p*-OMe, *p*-Cl, *p*-Br, *p*-OH, Naphtaline

Scheme 2 Transfer hydrogenation of aldehyde/ketone using mesoporous TTSA@Ni catalyst

to the SiO_2@TTSA nanocomposite (0.5 g), by stirring at room temperature for 4.5 h. The porous TTSA was then centrifuged, washed with water (50 mL), and dried in air.

2.4 Synthesis of TTSA@Ni NPs

An aqueous solution of $NiCl_2$-$6H_2O$ (2 mL, 1 M) was added to the preapared support (0.1 g) and refluxed for 3 h. The Ni^{2+} ions were subsequently reduced over aqueous $NaBH_4$ solution (12 mmol, 10 mL H_2O) and stirred for 4 h at room temperature. Finally, the TTSA@Ni nanocomposite so formed were isolated by centrifusion, rinsed with DI water: ethanol and dried under vacuum [24].

2.5 Preparation of benzyl alchohol derivatives using TTSA@Ni

In order to prepare a solution with pH of 3.2, a mixture of HCOOH-NEt_3 (1:0.7) was dissolved in water (1 mL). Then, the carbonyl compounds (1 mmol) and 0.03 g of TTSA@Ni nanocomposites were added to the above solution and stirred at 80 °C. After completion of the reaction as indicated by TLC (*n*-hexane/ethyl acetate, 10:3), mesoporous TTSA@Ni were separated via centrifusion. The product was then extracted out in excess ethyl acetate. The combined organic layer was rinsed with brine, dried over anhydrous Na_2SO_4, concentrated and finally in some cases column purified to afford the desired pure products.

3 Result and discussion

3.1 Analysis of catalyst characterization data

TTSA@Ni nanocomposite, being prepared following a post-synthetic modification approach, was analyzed over different techniques like FT-IR, FE-SEM, EDX, atomic mapping, ICP-OES, TEM, and XRD to have a detailed idea of its physical and chemical features.

In order to validate the stepwise formation of the nanocomposite, a comparison of SiO_2@TTSA (A), porous TTSA (B), TTSA@Ni (C), have been presented in Fig. 1. Figure 1A displays the characteristic peaks of N–H and NH_2 bond at 3200–3400 cm^{-1}. Also, some additional peaks are observed at 1172 and 1412 cm^{-1} corresponding to SO_2 bands. Moreover, the vibrations for C = S and C = N were found at 1689 and 1667 cm^{-1} respectively (Fig. 1A). Moreover, the adsorption of SiO_2@TTSA displayed absorption vibrational band at 1035 cm^{-1}, attributed to the Si–O stretching of silica nanoparticles. After silica etching procedure, this peak was not observed in the FT-IR spectra of the porous TTSA (Fig. 1B). In the next intermediate, i.e., TTSA@Ni nano composite (Fig. 1C), after interaction of Ni NPs with prepared support,

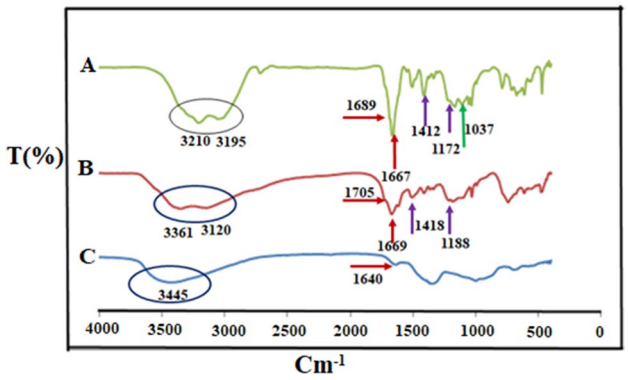

Fig. 1 FT-IR spectrum of SiO_2@TTSA NPs (**A**), Porous TTSA (**B**), TTSA@Ni nanocomposite (**C**)

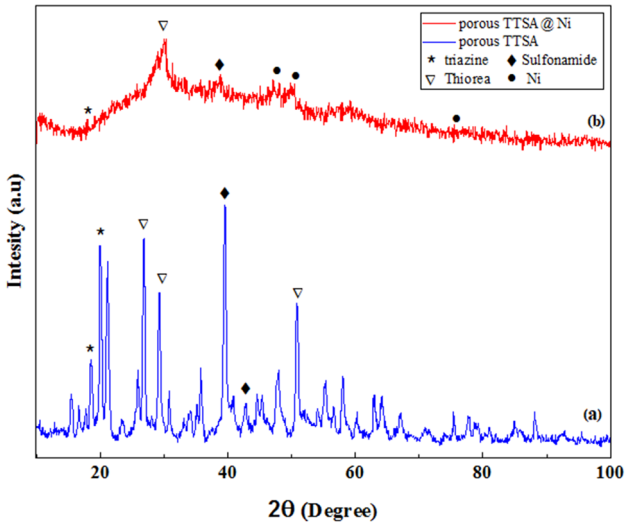

Fig. 2 XRD pattern of porous TTSA (**a**), TTSA@Ni (**b**)

the C = N peaks shifted from 1669 cm^{-1} to 1640 cm^{-1}. The observed shift peaks displayed the successful interaction of Ni owing to strong chelation with the polar functions groups.

The XRD pattern of synthesized porous TTSA and TTSA@Ni nanocomposite are shown in Fig. 2. The diffraction peaks in a range of 2θ angle at about 17.4°, 36.80°, 20° (due to the triazine group), 23.25° and 52° (due to the thiourea group), 40°and 45° (due to sulfonamide groups) confirmed the successful formation of crystal structure of porous TTSA (Fig. 2a).

The XRD pattern of TTSA@Ni nanocomposite is shown in Fig. 2b. The diffraction peaks in a range of 2θ angle 45°, 53° and 78° confirms the formation of Ni NPs and indicates that immobilization of Ni NPs lead to the formation of amorphous structure.

The morphology of SiO_2 nanoparticles was characterized with FE-SEM analysis (Fig. 3). The FE-SEM of SiO_2 NPs

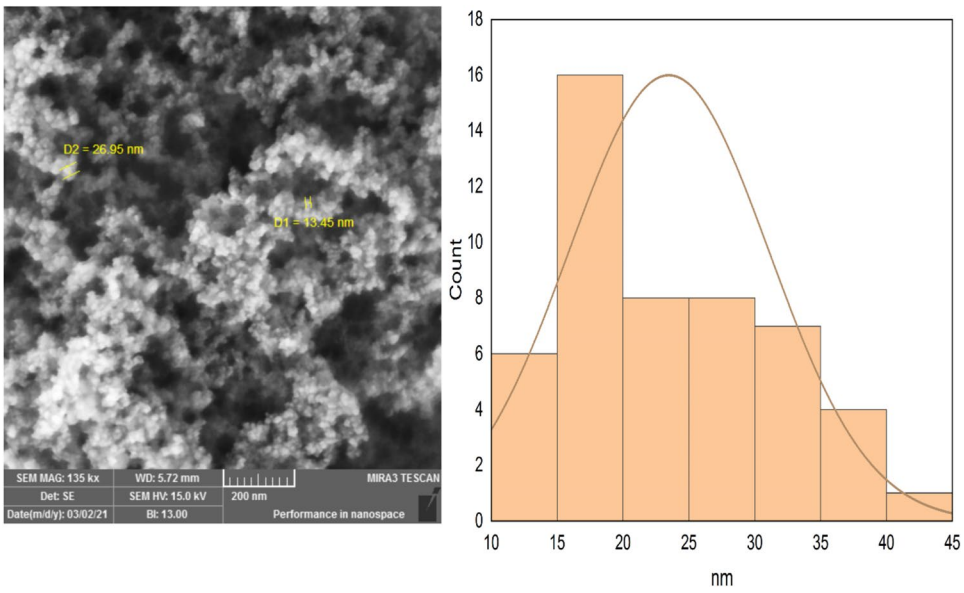

Fig. 3 FE-SEM image of SiO_2 NPs and the size distributions of SiO_2 NPs

showed spherical shaped Si NPs with mean size 10–25 nm. Moreover, the size distribution histogram of these nanoparticles confirms that their size average diameter is less than 25 nm.

FE-SEM analysis of porous TTSA and TTSA@Ni nanocomposite was performed to determine its surface morphology, porosity and particle size (Fig. 4). Mesoporous structure of TTSA indicated the effect of silica template method as an important factor on the porosity of the support (Fig. 4A). The detailed morphology, particle size and shape of TTSA@Ni showed the distribution of spherical shaped Ni NPs with mean size 25–35 nm on the surface of porous TTSA substrate (Fig. 4B).

To have a knowledge of the more detailed internal structure TEM analysis was carried out of the nanostructure. It clearly exhibits the quasi-spherical particles in nanometer range. (Fig. 5).

To confirm the presence of the elements on the nanocomposite, EDX and elemental mapping analysis was also performed. Figure 6 showing the EDX pattern, confirms the presence of Ni, O, S, C and N as the constituting elements. During elemental mapping, a section of the SEM image was scanned by X-ray and the outcomes are depicted in Fig. 7. The uniform dispersion of the composing atoms over the whole matrix can be clearly observed. The Ni content was measured by ICP-OES, to be 1.794 mmol g^{-1}.

The Brunauer–Emmett–Teller (BET) surface areas is determined by N_2 adsorption–desorption (Fig. 8). It is found the surface areas for porous TTSA is 31.77 $m^2\ g^{-1}$ and total pore volume is 0.07 $cm^3\ g^{-1}$ [25].

In order to investigate the amphiphilicity of the prepared catalyst, we used contact angle measurements. In this sense, Fig. 9 illustrates the contact angles of TTSA@Ni for both water and oil droplets. The obtained the contact angle

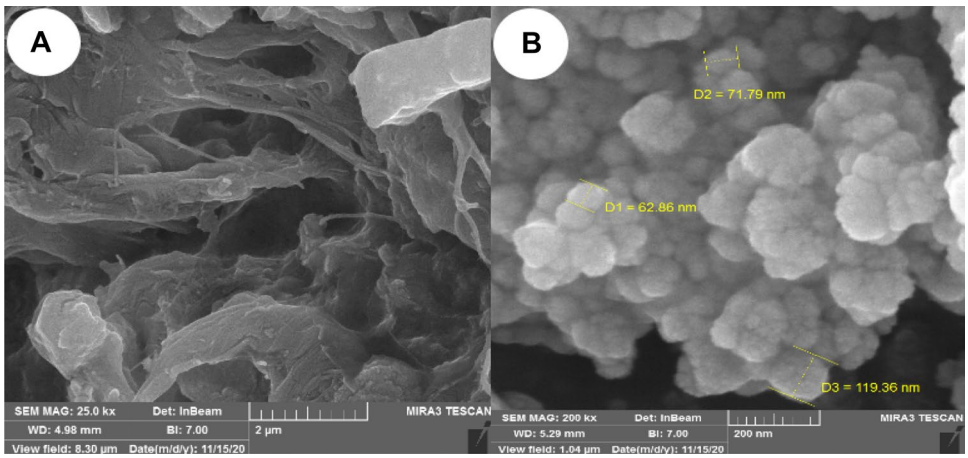

Fig. 4 FE-SEM photographs of porous TTSA (**A**) TTSA@Ni (**B**)

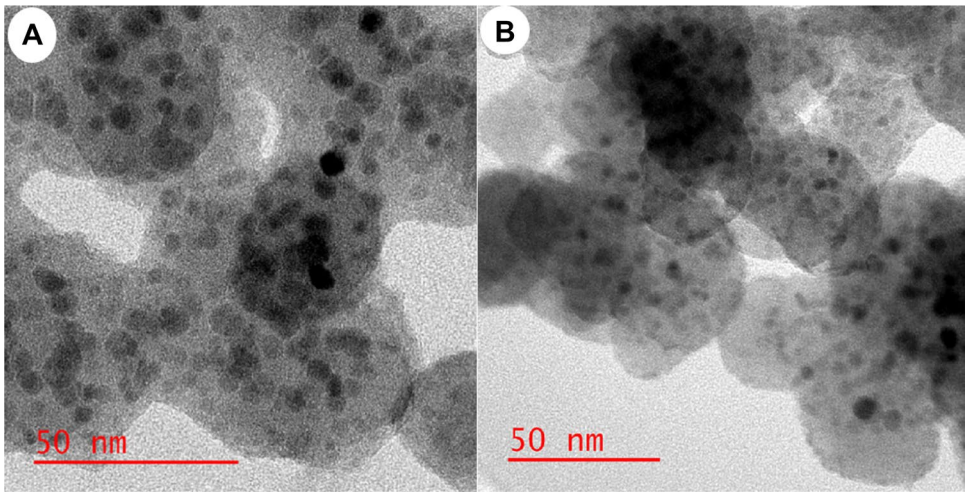

Fig. 5 HR-TEM images of TTSA@Ni with the scale bar of 50 nm

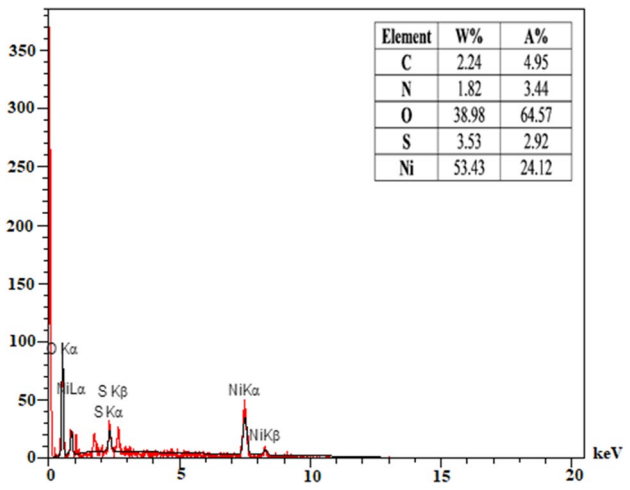

Fig. 6 EDX spectrum of TTSA@Ni NPs

between TTSA@Ni and water (below 90°) revealed that hydrophilicity of the prepared catalyst (Fig. 9A). Moreover, a rapid adsorption of the oil droplet was observed and the contact angle was about 0° (Fig. 9B).

TGA curve of TTSA@Ni NPs have been presented in Fig. 10, illustrated a small lose weight at 30–100 °C, which could be related to the physical absorption of water and organic solvents. After this, the weight decrease shown in the range of 230 – 600 °C indicates the degradation of polymer chains (Fig. 10).

3.2 Catalytic studies

We aimed at analyzing the optimization of reaction parameters, i.e. temperature, catalyst loading, hydrogen donor agent and solvent over TTSA@Ni the transfer hydrogenation of benzaldehyde (Table 1). As Table 1 shows, the reaction was not successful without the catalyst thus signifying their importance (entry 1). Initially, the effect of different hydride donor was investigated in the presence of 0.03 g (5.4 mol%) TTSA@Ni (entries 2–6). By using hydrogen donors such as formic acid, ammonium format, no further improvement in yield was observed (entries 2, 3). Thereafter, we optimized the formic acid/ammonium format in the reaction in various pH including 2.5, 3, and 3.5 (entries 4–6). It is worth nothing that pH is an important factor in the reaction progress and the excellent activity of the TTSA@Ni is vividly observed at a pH = 3 using HCOOH-$HCOONH_4$ (entry 4). Then, under various pH (entries 7–11), in the presence of HCOOH-NEt_3, the catalytic activity of TTSA@Ni was investigated. Interestingly, at a pH of 3.2, formic acid/triethyl amine resulted the best yield the shortest reaction time (entry 10). While studying the effect of temperature, we observed the reaction was sluggish at room temperature (entry 13). Again, at higher temperature there was no improvement in the reaction yields (entry 12), so the temperature was stabilized at 80 °C. Next, we checked the role of various solvents (entries 14–17) and solvent-free condition (entry 18). The best results were obtained using water as a reaction media (entry 10). Finally, the model reaction was examined in the presence of 0.05 g (9 mol%) (entry 19) and the optimal catalyst amount was found to be 5.4 mol% to push the reaction forward. In order to investigate the efficiency of TTSA@Ni, the model reaction was investigated in the presence of Ni NPs and we observed the reaction was sluggish (entry 20). In order to investigate the effect of base, the model reaction was investigate using HCOOH-NaOH and no reaction was occurred (entry 21).

On stabilizing the reaction conditions as discussed in Table 1, the next endeavor was to establish their scope and generality over a broad range of substrates, by reacting different aryl aldehydes and ketones over our developed catalyst (Table 2). Aromatic aldehydes having either electron-withdrawing groups (Cl, NO_2) (2b–c), electron-donating

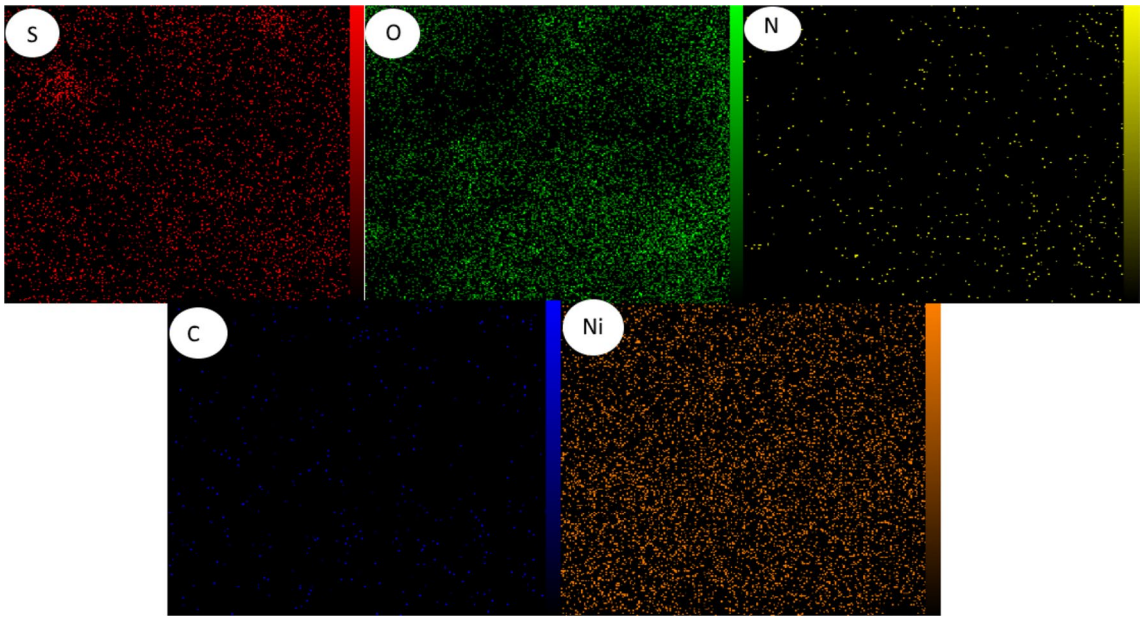

Fig. 7 Elemental mapping of TTSA@Ni shows the presence of C, N, O, S, and Ni atoms in the nanocomposite

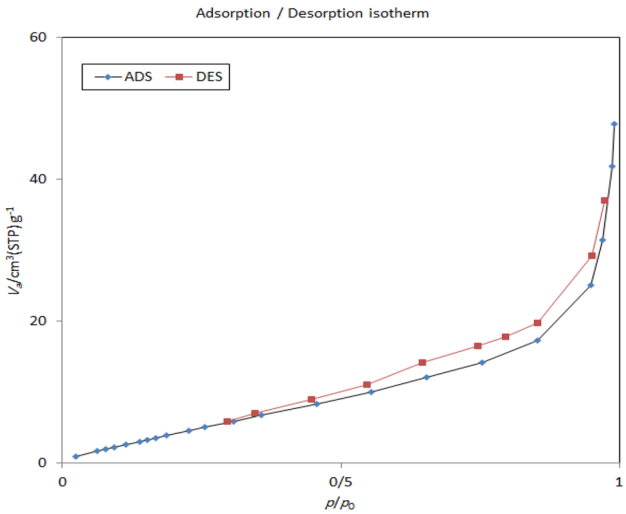

Fig. 8 BET measurment of TTSA polymer

groups (Me, OMe, $N(Me)_2$, F, OH) (2d–j) are all good substrates. Divers hetero aldehydes successfully reacted in good yields under set reaction conditions (2 k, 2 l, 2 m). Interstingly, terephthalaldehyde was found a good substrate with a yield of 89% (2n). Under the optimized reaction conditions, to further explore the extent and generality of present reaction procedure, a series of substituted acetophenone with electron-rich groups (Me, OMe, and OH) (2p, 2m and 2n), acetophenones with electron-deficient groups (Cl, Br) (2o, 2p) were converted efficiently into corresponding products in good to excellent yield. Other aryl ketone substrates (2r–2t) also successfully reacted in good yields under set reaction conditions.

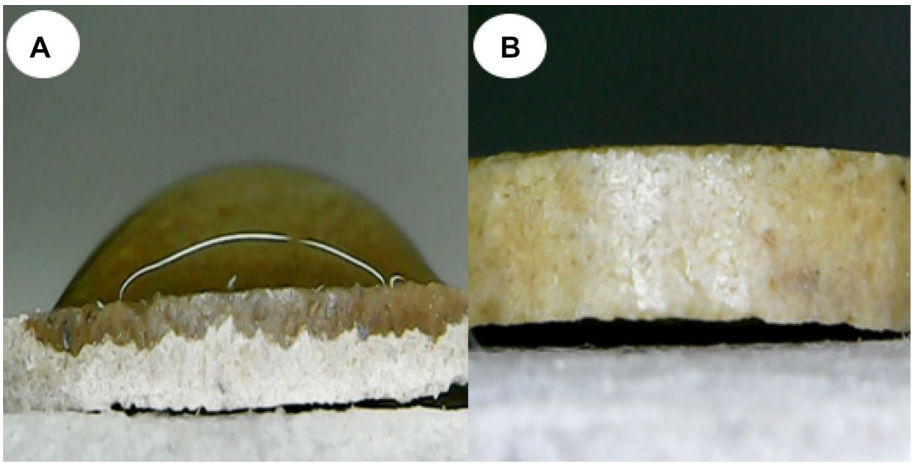

Fig. 9 Contact angles of TTSA@Ni, photograph of water (**A**) and oil droplet (**B**)

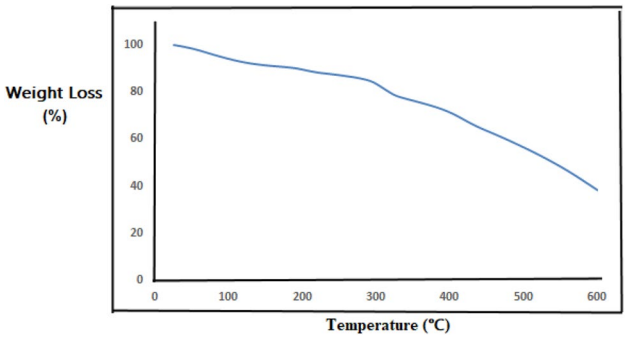

Fig. 10 TGA curve of TTSA@Ni nanocomposite

3.3 Proposed mechanism

A proposed mechanism for synthesizing benzyl alcohols catalysed by TTSA@Ni is presented in Scheme 3. It is assumed that during the course of reaction, TTSA@Ni nanocomposite has an important role in the decomposition of HCOOH that lead to hydride produce in the presence of triethyl amine. Finally, the desired benzyl alochohol was obtained through hydrogenation [2] (Scheme 3).

After the completion of model reaction under best optimized green reaction conditions, the nanocomposite TTSA@Ni was recovered easily and reused in subsequent six runs (Fig. 11). In the regeneration study, after each recycle, TTSA@Ni was separated out from the reaction mixture through centrifusion and washing with water: ethanol (20 mL). After each recycle, the product yield has been marginally decreased (98, 96, 94, 93, 88, 84), very little and insignificant change in the product yield has been noticed.

After 5 times, as FT-IR spectra show, the structure of the catalyst didn't significantly change (Fig. 12).

4 Conclusion

The aim of the present research was to examine the effect of silica NPs on the synthesis of mesoporous polysulfonamide-based catalyst. Mesoporous structure, amphiphilicity and numerous polar electron rich functions provide significant stability to the NPs by homogeneous and wide distribution over the matrix. TTSA@Ni nanocomposite was exploited in the synthesis of diverse benzyl alchohol derivatives by the reduction of aldehydes/ketones. The whole process can be considered as an ideal tool because synthesis of both nanocatalyst and desired products were achieved in environmentally friendly conditions and additionally, catalyst could be easily recovered and reused.

Table 1 Optimization of the reaction conditions

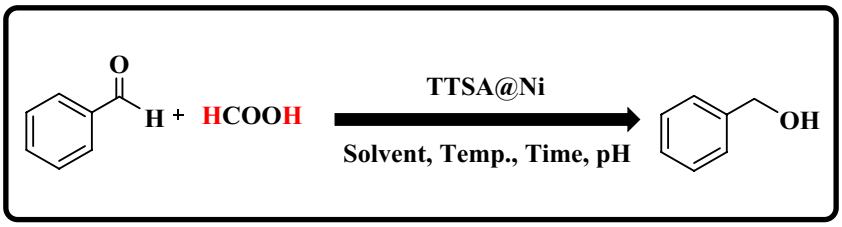

Entry	Cat. (g)	Hydrogen doner	Solvent	Temperature (°C)	Time (h)	Yield (%)[a]
1	–	HCOOH	H_2O	80	24	N.R.
2	0.03	HCOOH	H_2O	80	24	Trace
3	0.03	$HCOONH_4$	H_2O	80	12	50
4	0.03	HCOOH–$HCOONH_4$ (pH=3)	H_2O	80	6	80
5	0.03	HCOOH–$HCOONH_4$ (pH=2.5)	H_2O	80	8	72
6	0.03	HCOOH–$HCOONH_4$ (pH=3.5)	H_2O	80	6	76
7	0.03	HCOOH–NEt_3 (1:0.2, pH=1.5)	H_2O	80	6	40
8	0.03	HCOOH–NEt_3 (1:0.3, pH=2.0)	H_2O	80	6	60
9	0.03	HCOOH–NEt_3 (1:0.5, pH=2.5)	H_2O	80	3	84
10	0.03	HCOOH–NEt_3 (1:0.7, pH=3.2)	H_2O	80	0.5	98
11	0.03	HCOOH–NEt_3 (1:1, pH=3.7)	H_2O	80	0.5	94
12	0.03	HCOOH–NEt_3 (1:0.7, pH=3.2)	H_2O	60	0.05	88
13	0.03	HCOOH–NEt_3 (1:0.7, pH=3.2)	H_2O	R.T.	12	45
14	0.03	HCOOH–NEt_3 (1:0.7, pH=3.2)	EtOH	80	1	80
15	0.03	HCOOH–NEt_3 (1:0.7, pH=3.2)	H_2O:EtOH	80	1	85
16	0.03	HCOOH-NEt_3 (1:0.7, pH=3.2)	THF	80	24	Trace
17	0.03	HCOOH–NEt_3 (1:0.7, pH=3.2)	CH_3CN	80	24	50
18	0.03	HCOOH–NEt_3 (1:0.7, pH=3.2)	Solvent-free	80	24	60
19[b]	0.05	HCOOH–NEt_3 (1:0.7, pH=3.2)	H_2O	80	0.5	90
20[c]	0.05	HCOOH–NEt_3 (1:0.7, pH=3.2)	H_2O	80	5	55
21[d]	0.05	HCOOH-NaOH	H_2O	80	24	N.R

[a]Isolated yield

[b]The reaction was examined in the presence of 0.03 g of TTSA@Ni

[c]The reaction was examined in the presence of 0.03 g of Ni NPs

[d]The reaction was examined in the presence HCOOH–NaOH

Table 2 Reduction of different aldehydes and ketones to alcohols in the presence of TTSA@Ni nanocatalyst using formic acid-triethylamine as reducing agent[a]

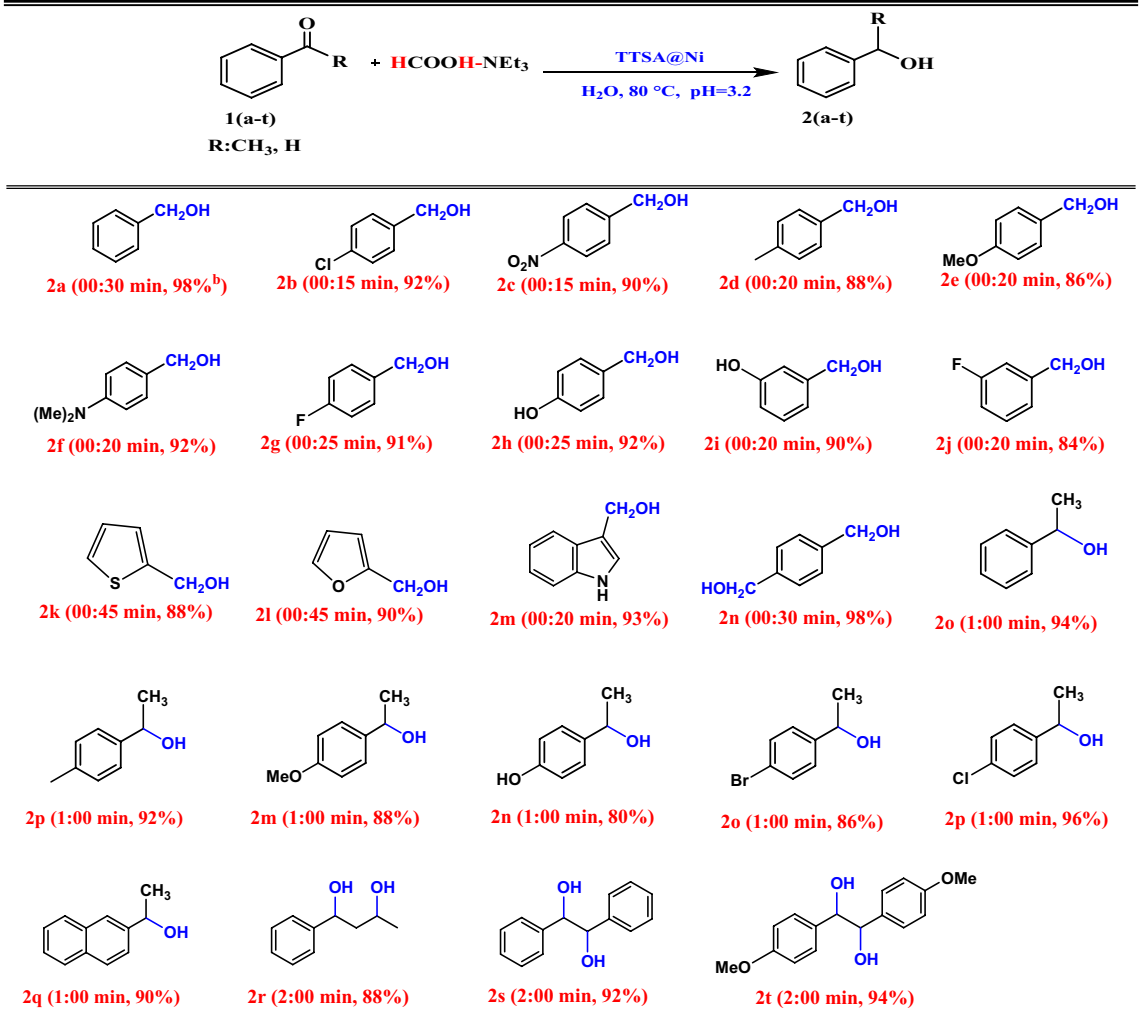

[a]Reaction condition: benzaldehyde or acetophenone derivatives (1 mmol), formic acid-triethyl amine (1: 0.7 mmol), TTSA@Ni (0.03 g), H_2O (1 mL), 80 °C

[b]Isolated yield

Scheme 3 Proposed reaction mechanism for the reduction of carbonyl compounds using TTSA@Ni catalyst

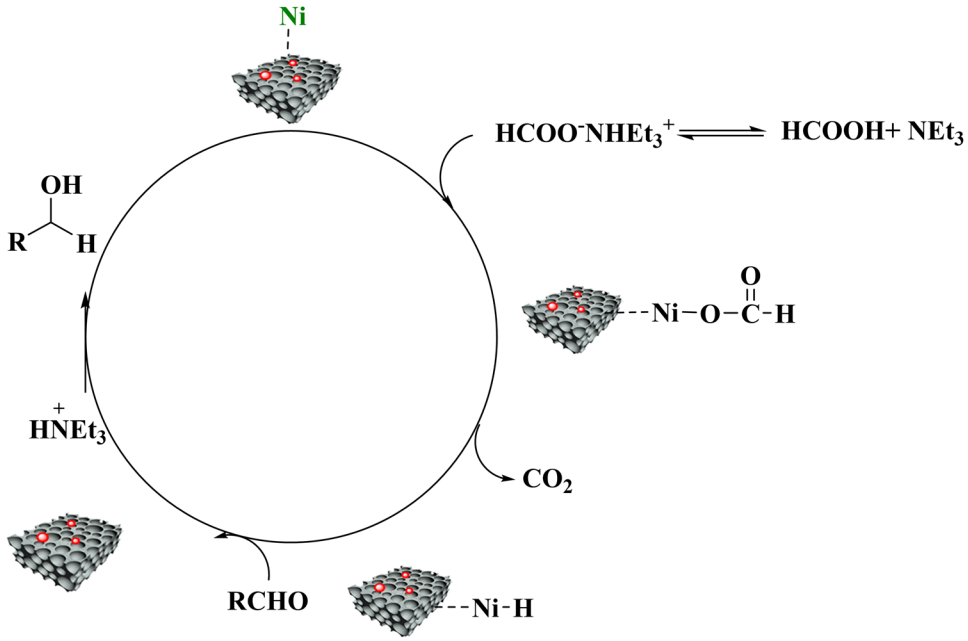

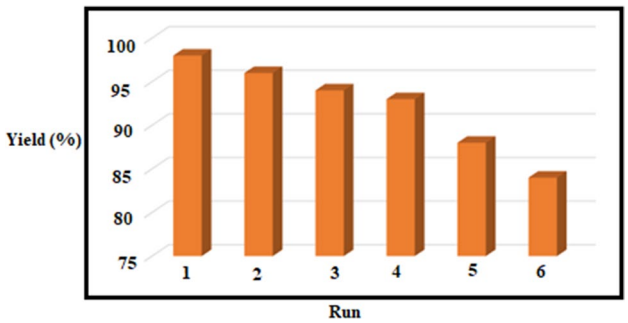

Fig. 11 Recycling of the TTSA@Ni for the reduction of benzaldehyde

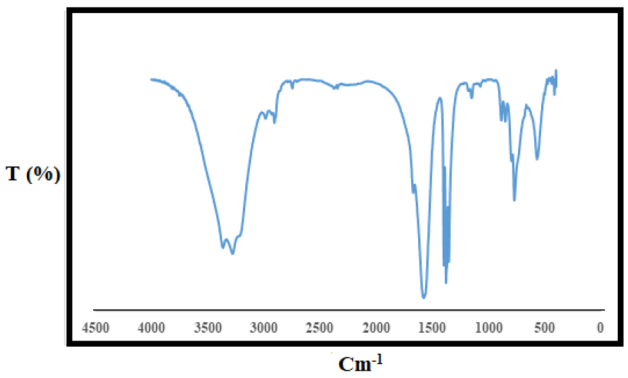

Fig. 12 FT-IR spectrum of the TTSA@Ni after the reaction

Supplementary Information The online version contains supplementary material available at https://doi.org/10.1007/s10934-021-01104-1.

Acknowledgements The authors would like to thank Bu-Ali Sina University, Center of Excellence Developmental of Environmentally Friendly Methods for Chemical Synthesis (CEDEFMCS) for financial supporting of this research.

References

1. H. Nur, S. Ikeda, B. Ohtani, J. Catal. **204**, 402–408 (2001)
2. F. Panahi, F. Haghighi, A. Khalafi-Nezhad, Appl. Organomet. Chem. (2020). https://doi.org/10.1002/aoc.5880
3. D. Mao, W. Yang, J. Xia, B. Zhang, Q. Song, Q. Chen, J. Catal. **230**, 140–149 (2005)
4. J. Tejero, F. Cunill, M. Iborra, F. Izquierdo, C. Fite, J. Mol. Catal. Chem. **182**, 541–554 (2002)
5. K. Manabe, S. Iimura, M. Xiang, S. Kobayashi, J. Am. Chem. Soc. **124**, 11971–11978 (2002)
6. A. Maleki, R. Taheri-Ledari, R. Ghalavand, R. Firouzi-Haji, J. Phys. Chem. Solids. **136**, 109200–109208 (2020)
7. M. Mahmoodi, A. Bamoniri, A. Taherpour, J. Heterocycl. Chem. **57**, 1–14 (2020)
8. S. Hemmati, M. Heravi, B. Karmakar, H. Veisi, J. Mol. Liq. **319**, 114302–114311 (2020)
9. P. Ghasemi, M. Yarie, M.A. Zolfigol, A.A. Taherpour, M. Torabi, ACS Omega **5**, 3207–3217 (2020)
10. Y. Lei, M. Zhang, Q. Li, Y. Xia, G. Leng, Polymers **11**, 2091 (2019)
11. Y. Lei, Y. Wan, G. Li, X.Y. Zhou, Y. Gu, J. Feng, R. Wang, Mater. Chem. Front. **11**, 1541–1549 (2017)
12. S. Babaee, M. Zarei, M.A. Zolfigol, S. Khazalpour, M. Hasani, U. Rinner, R. Schirhagl, N. Norouzi, S. Rostamnia, RSC Adv. **11**, 2141–2157 (2021)
13. M. Manzoli, E.C. Gaudino, G. Cravotto, S. Tabasso, R.B. Nasir Baig, E. Colacino, R.S. Varma, ACS Sustain. Chem. Eng. **7**, 5963–5974 (2019)

14. M. Dajek, R. Kowalczyk, P.J. Boratynski, Catal. Sci. Technol. **8**, 4358–4363 (2019)
15. R. Ghorbani-Vaghei, S. Alavinia, N. Sarmast, Appl. Organomet. Chem. **32**, e4038 (2018)
16. R. Ghorbani-Vaghei, S. Alavinia, Z. Merati, V. Izadkhah, Appl. Organomet. Chem. **32**, e4127 (2018)
17. S. Alavinia, R. Ghorbani-Vaghei, J. Phys. Chem. Solids. **146**, 109573–109584 (2018)
18. A. Fatehi, R. Ghorbani-Vaghei, S. Alavinia, J. Mahmoodi, Chem. Select. **5**, 944–951 (2020)
19. F. Hamidi Dastjerdi, R. Ghorbani-Vaghei, S. Alavinia, Catal. Lett. **150**, 3514–3522 (2020)
20. N. Shekarlab, R. Ghorbani-Vaghei, S. Alavinia, Appl. Organomet. Chem. **34**, e5918 (2020)
21. S. Solgi, R. Ghorbani-Vaghei, S. Alavinia, J. Porous. Mater. **28**, 289–298 (2020)
22. S. Alavinia, R. Ghorbani-Vaghei, New J. Chem. **44**, 13062–13073 (2020)
23. W. Stöberand, A. Fink, J. Colloid. Interf. Sci. **26**, 62–69 (1968)
24. S. Khan, A. Ghatak, S. Bhar, Tetrahedron Lett. **56**, 2480–2487 (2015)
25. S.W. Sing, W. Kenneth, Adsorp. Sci. Technol. **22**, 773–782 (2004)